SOLIDS
AND LIQUIDS

Spectral Properties of Waves in Superlattices with 2D and 3D Inhomogeneities

V. A. Ignatchenko and D. S. Tsikalov

L.V. Kirensky Institute of Physics, Siberian Branch, Russian Academy of Sciences, Krasnoyarsk, 660036 Russia

e-mail: vignatch@iph.krasn.ru

Received May 11, 2010

Abstract—We investigate the dynamic susceptibility and one-dimensional density of states in an initially sinusoidal superlattice containing simultaneously 2D phase inhomogeneities simulating correlated roughnesses of superlattice interfaces and 3D amplitude inhomogeneities of the superlattice layer materials. The analytic expression for the averaged Green's function of the sinusoidal superlattice with two phase inhomogeneities is derived in the Bourret approximation. It is shown that the effect of increasing asymmetry in the peak heights of dynamic susceptibility at the Brillouin zone boundary of the superlattice, which was discovered earlier [15] upon an increase in root-mean-square (rms) fluctuations, also takes place upon an increase in the correlation wavenumber of inhomogeneities. However, the peaks in this case also become closer, and the width and depth of the gap in the density of states decrease thereby. It is shown that the enhancement of rms fluctuations of 3D amplitude inhomogeneities in a superlattice containing 2D phase inhomogeneities suppresses the effect of dynamic susceptibility asymmetry and leads to a slight broadening of the gap in the density of states and a decrease in its depth. Targeted experiments aimed at detecting the effects studied here would facilitate the development of radio-spectroscopic and optical methods for identifying the presence of inhomogeneities of various dimensions in multilayer magnetic and optical structures.

1. INTRODUCTION

In the last two decades, theoretical studies have been developed intensely on the effect of inhomogeneities in the geometrical structure of initially periodic superlattices on the spectral properties of waves of various nature or electronic excitations propagating in such media. For this purpose, computer simulation methods were mainly employed. In these studies, one-dimensional (1D) geometrical disorder was considered as a rule, which was simulated either by violation of periodicity in the arrangement of the layers of various materials forming superlattices or by random deviations in the thickness of these layers. Various analytical approaches were also developed. The Green's's function method was used for investigating such structures in [1–3]. In the proposed model [4], the method of averaged Green's functions was proposed for approximate analysis of geometrical 1D, 2D, and 3D disorder in superlattices with a sinusoidal profile of the dependence of a material parameter on the z coordinate in the initial state (assuming that the z axis is perpendicular to the plane of the layers in the superlattice). Inhomogeneities in such a superlattice were simulated by introducing a random phase $u(\mathbf{x})$ into the harmonic function, which can be a function of one ($\mathbf{x} = \{z\}$), two ($\mathbf{x} = \{x, y\}$), or three coordinates ($\mathbf{x} = \{x, y, z\}$). In this model, the position of zeros of the harmonic function simulates the position of boundaries

(interfaces) between superlattice layers. The 1D phase $u_1 = u_1(z)$ describes random displacements of these interfaces from their initial periodic arrangement (or, equivalently, the random thickness of the layers in the superlattice). Like the 2D phase $u_2 = u_2(x, y)$, the 3D phase $u_3 = u_3(x, y, z)$ describes a random deformation (roughness) of the interfaces in the xy plane. In this case, 2D phase inhomogeneities simulate deformations identical for all interfaces because such inhomogeneities have an infinitely large correlation radius along the z axis. The correlation radius of 3D phase inhomogeneities is finite both in the xy plane and along the z axis. In the general case, 3D inhomogeneities exhibit anisotropic correlation properties and have different correlation radii in the xy plane and along the z axis. Therefore, such inhomogeneities can simulate various actual situations. In particular, if the correlation radius of 3D phase inhomogeneities along the z axis is much smaller than the layer thickness in the superlattice, roughnesses of the interfaces are stochastically independent even at adjacent layers. In the opposite case, when the correlation radius along the z axis is larger than the thickness of not only the layers, but of the entire superlattice also, correlated roughnesses are simulated in our model by 2D phase inhomogeneities.

The only characteristic describing a random medium and appearing in the expression for the averaged Green's function is correlation function $K(\mathbf{r})$ depending on distance $\mathbf{r}$ between two points of the medium: $\mathbf{r} = \mathbf{x} - \mathbf{x}'$. For this reason, the first part of the problem is reduced to determining function $K(\mathbf{r})$ for the superlattice with certain inhomogeneities, while the second part of the problem involves the extraction of spectra characteristics from the expression for the Green's function containing this correlation function with the help of standard approximate methods. To determine correlation function $K(\mathbf{r})$ of a superlattice, the random spatial modulation (RSM) method was developed in [4], which is a generalization of the well-known method for calculating the temporal correlation function for random frequency (phase) modulation of a radio signal [5, 6] to the case of spatial (three-dimensional in the general case) modulation of the superlattice period. The advantage of this method is the fact that the form of correlation function $K(\mathbf{r})$ is not postulated, but is derived from the most general assumptions concerning the type of random spatial modulation $u = u(\mathbf{x})$ of the superlattice period. It was shown that the form of function $K(\mathbf{r})$ in the general case considerably depends on the dimensionality of inhomogeneities and on the structure of interfaces between the layers.

The RSM method was subsequently generalized to a superlattice with a rectangular profile [7] and with an arbitrary thickness of interfaces [8]. To derive correlation function $K(\mathbf{r})$ in this method, it is necessary to postulate the form of correlation function $K_u(\mathbf{r})$ of the gradient of function $u(\mathbf{x})$. The analytic expressions obtained for $K(\mathbf{r})$ have a complex form determined to a considerable extent by the form of $K_u(\mathbf{r})$. It turned out, however, that the asymptotic form of function $K(\mathbf{r})$ for small as well as large values of $|\mathbf{r}|$ is independent of the form of function $K_u(\mathbf{r})$ if the latter exhibits a rapid decay of correlations (e.g., exponential or Gaussian decay). It was shown that the spectral properties of waves are mainly determined by the asymptotic properties of correlation function $K(\mathbf{r})$ of the superlattice. Therefore, this method makes it possible to describe geometrical inhomogeneities of different dimensions using a unified approach. The knowledge of function $K(\mathbf{r})$ for various types of superlattice and various dimensions of inhomogeneities permitted the use of averaged Green's function to study the effect of 1D and 3D phase inhomogeneities for isotropic as well as anisotropic correlations, and also the joint effect of 1D and 3D inhomogeneities (both stochastically independent and coupled by cross-correlations with one another) on the spectrum, decay, and dynamic susceptibility of waves in superlattices (see [9] and references [21−27] therein).

The spectral properties of superlattices with 2D phase inhomogeneities have not yet been studied as comprehensively. A modification of the dispersion relation and the decay of waves in a sinusoidal superlattice associated with 2D inhomogeneities were briefly considered in [4] using the two-zone model. It was shown that in contrast to 1D and 3D inhomogeneities, the decay associated with 2D inhomogeneities is observed only on the spectral branch corresponding to the second Brillouin zone, while the frequency of the first zone remains real-valued. It should be noted that the situation described by 2D phase inhomogeneities is not as exotic. Such a situation may take place in actual practice when roughness of interfaces results from the roughness of the surface of the substrate on which the superlattice layers are deposited. In this case, random roughness in the xy plane can be repeated almost in phase on the surface of each newly deposited layer, and the superlattice can be approximately described by a correlation function of 2D inhomogeneities with a finite correlation radius in the xy plane of the layers and an infinite correlation radius along the z axis.

The small-angle X-ray scattering technique [10] is the most informative method for studying inhomogeneities in the structure of superlattices and their interfaces. From the very outset of experiments with semiconductor superlattices, this method revealed singularities in some scattering spectra, which were attributed to correlations between the roughnesses of different interfaces in the superlattice [11]. In [12], a consistent theory of small-angle X-ray scattering in a superlattice was developed taking into account the correlation of roughnesses of interfaces. The spectral effects caused by correlations such as peculiarities in the formation of resonance peaks in the diffuse scattering region and the formation of strips in the radiation intensity distribution in the plane of wavevectors $k_x k_z$ were described. Subsequently, these effects were studied in detail theoretically and experimentally (see, for example, [13, 14] and the literature therein).

In the model considered here, an increase in the correlation radius in the direction of the z axis indicates a gradual approach to 2D inhomogeneities. In this connection, it was important to reveal the effects in the spectrum of spin and optical waves (apart from the effect of vanishing of the decay of waves in the first Brillouin zone of the superlattice established in [4]), which are associated with mutual correlations between inhomogeneities of the interfaces in this limiting case. The dynamic susceptibility (the Green's function) of a superlattice with 2D phase inhomogeneities was studied in [15]. It was shown that the susceptibility peaks at the boundary of the first Brillouin zone of the superlattice become asymmetric upon an increase in the intensity of such inhomogeneities: the peak corresponding to the low-frequency edge of the band gap is displaced to the center of the band without changing its width, while the peak corresponding to the high-

frequency edge of the band gap is broadened and its height sharply decreases until it disappears completely. Such asymmetry is not observed for 1D and 3D inhomogeneities and is a consequence of peculiarities in the energy conservation law of the incident wave and the waves scattered from 2D inhomogeneities. It was shown in [16] that this effect must take place at the boundaries of all odd Brillouin zones of a superlattice containing 2D inhomogeneities. In these publications, Green's function $G(\nu, \mathbf{k})$ was determined by numerical integration for fixed values of wavenumber k: $k = k_r \equiv q/2$ (where $q = 2\pi/L$, L being the period of the superlattice) at the boundary of the first Brillouin zone in [15] or at the boundaries of the next odd Brillouin zones for $k = (2n-1)q/2$ in [16] ($n = 1, 2, 3, ...$).

This aim of this study is to derive an analytic expression for the averaged Green's function of the superlattice in the Bourret approximation [17] and its analysis based on the dynamic susceptibility and 1D density of states of superlattices with 2D phase inhomogeneities, as well as with 2D phase inhomogeneities coexisting with 3D amplitude inhomogeneities simulating inhomogeneities in the layers of the superlattice material.

2. MODEL AND METHOD

In the case considered here, the coordinate dependence $A(\mathbf{x})$, where $\mathbf{x} = \{x, y, z\}$, of a material parameter of the superlattice can be represented in the form

$$A(\mathbf{x}) = A + (\Delta A)_a \rho_a(\mathbf{x}) + (\Delta A)_p \rho_p(\mathbf{x}), \qquad (1)$$

where A is the mean value of the parameter; $(\Delta A)_a$ and $(\Delta A)_p$ are the amplitude and phase rms deviations, respectively; and $\rho_a(\mathbf{x})$ and $\rho_p(\mathbf{x})$ are centered ($\langle \rho_i(\mathbf{x}) \rangle = 0$) and normalized ($\langle \rho_i^2(\mathbf{x}) \rangle = 1$) functions, $i = a, p$. Function $\rho_a(\mathbf{x})$ is a random homogeneous function simulating inhomogeneities of the material of the layers in the superlattice. Function $\rho_p(\mathbf{x})$ describes both the periodic dependence of the parameter along the z axis of the superlattice and the random spatial modulation of this parameter, which in the case considered here is a function of two coordinates (x and y). The random component of this function simulates the deformation of the surface of the interfaces, which is identical for all interfaces. We assume that random functions $\rho_a(\mathbf{x})$ and $\rho_p(\mathbf{x})$ are assumed here to be stochastically independent.

We consider a superlattice with a sinusoidal dependence of the material parameter on the z coordinate in the initial state in the absence of random inhomogeneities. Following [15], we represent function $\rho_p(\mathbf{x})$ in the form

$$\rho_p(\mathbf{x}) = \sqrt{2} \cos\{q[z - u(x, y)] + \psi\}, \qquad (2)$$

where random function $u(x, y)$ simulates 2D deformations of the interfaces in the superlattice. Coordinate-

independent phase ψ is characterized by a uniform distribution on the interval $(-\pi, \pi)$.

The wave equation for the temporal Fourier transformant in the superlattice can be written in the form

$$\nabla^2 m + \left[\nu - \frac{\Lambda_a}{\sqrt{2}} \rho_a(\mathbf{x}) - \frac{\Lambda_p}{\sqrt{2}} \rho_p(\mathbf{x}) \right] m = 0, \qquad (3)$$

where function $m = m(\mathbf{x}, \omega)$ and parameters ν and Λ_i are different for waves of different origins. For spin waves, Eq. (3) corresponds to a ferromagnetic superlattice with a nonuniform magnetic anisotropy parameter $\beta(\mathbf{x})$ ($A = \beta$, $(\Delta A)_i = (\Delta\beta)_i$ in formula (1)) in the situation when the directions of external magnetic field $\mathbf{H}$, constant component $\mathbf{M}_0$ of magnetization $\mathbf{M}$, and the magnetic anisotropy axis coincide with the direction of the z axis of the superlattice. In this case, we have

$$m = M_x + iM_y, \quad \nu = \frac{\omega - \omega_0}{\alpha g M_0}, \quad \Lambda_i = \frac{\sqrt{2}(\Delta\beta)_i}{\alpha},$$

where ω is the frequency, $\omega_0 = g[H + (\beta - 4\pi)M_0]$ is the frequency of the uniform ferromagnetic resonance, g is the gyromagnetic ratio, and α is the exchange constant. For elastic waves in the scalar approximation, for a superlattice with nonuniform density $p(\mathbf{x})$ of the medium ($A = p$, $(\Delta A)_i = (\Delta p)_i$), we have

$$\nu = \left(\frac{\omega}{s} \right)^2, \quad \Lambda_i = \frac{\sqrt{2}\omega^2(\Delta p)_i}{ps^2},$$

where s is the velocity of elastic waves. For electromagnetic waves in the same approximation in a medium with nonuniform permittivity $\varepsilon(\mathbf{x})$ ($A = \varepsilon$, $(\Delta A)_i = (\Delta\varepsilon)_i$), we have

$$\nu = \varepsilon\left(\frac{\omega}{c} \right)^2, \quad \Lambda_i = \sqrt{2}(\Delta\varepsilon)_i\left(\frac{\omega}{c} \right)^2,$$

where c is the velocity of light.

The Fourier transform of the averaged Green's function for Eq. (3) has the form

$$G(\nu, \mathbf{k}) = \frac{1}{(2\pi)^3} \frac{1}{\nu - k^2 - M_a(\nu, \mathbf{k}) - M_p(\nu, \mathbf{k})}, \qquad (4)$$

where $M_a(\nu, \mathbf{k})$ and $M_p(\nu, \mathbf{k})$ are the mass operators of amplitude and phase inhomogeneities, respectively; in the Bourret approximation, these operators can be represented in the form [18]

$$M_i(\nu, \mathbf{k}) = -\frac{\Lambda_i^2}{8\pi} \int \frac{K_i(\mathbf{r})}{|\mathbf{r}|} \times \exp[-i(\mathbf{kr} + \sqrt{\nu}|\mathbf{r}|)]d\mathbf{r}, \qquad (5)$$

where $K_i(\mathbf{r})$ are the correlation functions of amplitude ($i = a$) and phase ($i = p$) inhomogeneities, which are defined as

$$K_i(\mathbf{r}) = \langle \rho_i(\mathbf{x})\rho_i(\mathbf{x}+\mathbf{r}) \rangle. \tag{6}$$

The correlation function of isotropic 3D amplitude inhomogeneities has the form

$$K_a(\mathbf{r}) = \exp(-k_3|\mathbf{r}|), \tag{7}$$

where $k_3 = r_3^{-1}$ is the correlation wavenumber for 3D inhomogeneities and r_3 is the correlation radius of these inhomogeneities. The exact form of the correlation function for 2D phase inhomogeneities was determined in [15]:

$$K_p(\mathbf{r}) = \cos(qz)\exp\left[-\frac{Q(r_\perp)}{2}\right], \tag{8}$$

where

$$Q(r_\perp) = 4\gamma_2^2\{E_1(k_2 r_\perp) + \ln(k_2 r_\perp C) \\ + \exp(-k_2 r_\perp) - 1\}, \tag{9}$$

$r_\perp = \sqrt{r_x^2 + r_y^2}$, $C \approx 1.78$ is the Euler constant,

$$E_1(z) = \int_z^\infty \frac{e^{-t}}{t}dt$$

is the integral exponential function, and γ_2 and $k_2 = r_2^{-1}$ are the rms fluctuation and the correlation wavenumber, respectively, of 2D phase inhomogeneities (r_2 is their correlation radius). In the limiting cases of large and small values of $r_\perp$, expression (9) assumes the form

$$Q(\mathbf{r}) = \gamma_2^2\begin{cases} k_2^2 r_\perp^2, & k_2 r_\perp \ll 1 \\ 4\ln(k_2 r_\perp C/e), & k_2 r_\perp \gg 1, \end{cases} \tag{10}$$

where $e \approx 2.72$ is the base of the natural logarithm.

Expression (8) is too cumbersome. For this reason, the following expression approximating this function was proposed in [15]:

$$K_p(\mathbf{r}) = \cos(qr_z)\left(1 + \frac{C^2}{e^2}k_2^2 r_\perp^2\right)^{-\gamma_2^2}. \tag{11}$$

It was shown that model correlation function (11) correctly describes the exact correlation function in the entire range of $r_\perp$ and has an asymptotic form coinciding with the asymptotic form of the exact function both for $k_2 r_\perp \ll 1$ and for $k_2 r_\perp \gg 1$. The latter requirement plays a major role in the selection of the approximating correlation function since it was shown earlier (for 1D and 3D inhomogeneities as well as for their mixture) that the spectral properties of waves are mainly determined by the asymptotic form of the correlation function for inhomogeneities for $r \longrightarrow \infty$.

Mass operator M_a for isotropic 3D amplitude inhomogeneities described by correlation function (7) in the Burre approximation has the form [19]

$$M_a = \frac{\Lambda_a^2}{2}\frac{1}{\left(\sqrt{\nu} - ik_3\right)^2 - k^2}. \tag{12}$$

Mass operator M_p for 2D phase inhomogeneities described by correlations function (11) was analyzed in [15]. After passage to the spherical system of coordinates in expression (5) with the polar axis directed along the z axis, integration was performed over azimuth angle φ and the modulus of radius vector $\mathbf{r}$. As a result, we obtained a one-dimensional integral of a complex integrand with respect to polar angle θ, which was evaluated numerically. Such an algorithm for solving the problem was admissible for analysis of Green's function $G(\nu, \mathbf{k})$ for fixed values of wavenumber k: $k = k_r \equiv q/2$ at the boundary of the first Brillouin zone in [15] or $k = (2n - 1)q/2$ at the boundaries of the next odd Brillouin zones in [16]. For our purposes, we must know Green's function $G(\nu, k)$ for each value of wavenumber k because the density of states is evaluated by integrating the imaginary part of this function with respect to k. The method for calculating M_p used in [15, 16] is hardly applicable for these purposes because it involves vast numerical calculations. For this reason, we use another approach enabling us to obtain an analytic expression for $M_p(\nu, k)$ for 2D phase inhomogeneities.

3. MASS OPERATOR FOR 2D PHASE INHOMOGENEITIES

We pass to a cylindrical system of coordinates in expression (5), introducing the following simplifying notation:

$$\rho = r_\perp \equiv \sqrt{r_x^2 + r_y^2}, \quad z = r_z. \tag{13}$$

Integrating with respect to azimuth angle φ and representing $\cos qz$ in expression (11) as the sum of two exponentials, we can write the mass operator for 2D phase inhomogeneities in the form

$$M_p(\nu, k) = M_p^-(\nu, k) + M_p^+(\nu, k), \tag{14}$$

where

$$M_p^\pm(\nu, k) = -\frac{\Lambda_p^2}{8}\int_0^\infty \mathcal{K}(\rho)\mathfrak{I}^\pm(\nu, k, \rho)\rho\, d\rho. \tag{15}$$

Here, $k = k_z$ and $\mathcal{K}$ is the decreasing part of correlation function (11),

$$\mathcal{K}(\rho) = \left(1 + \frac{C^2}{e^2}k_2^2\rho^2\right)^{-\gamma_2^2}, \tag{16}$$
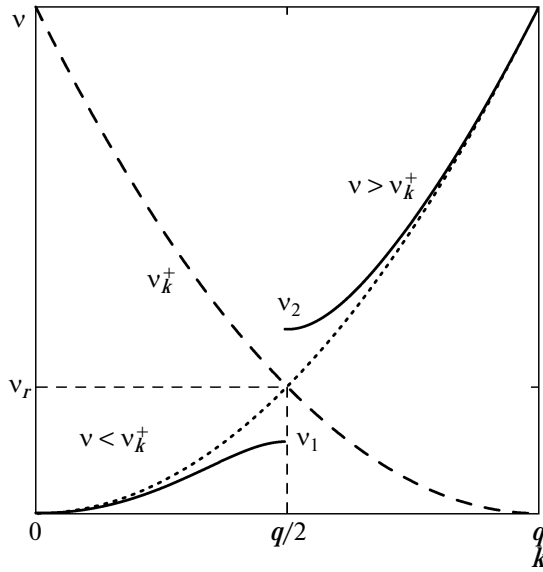
Fig. 1 Schematic diagram of the dispersion relation for spin waves for an ideal superlattice (solid curves $\nu < \nu_k^+$ and $\nu > \nu_k^+$ for the first and second Brillouin zone of the superlattice, respectively) and for a homogeneous ferromagnet (dotted curve, $\nu = k^2$). The dashed curve shows the auxiliary branch $\nu_k^+ = (k - q)^2$.

and functions $\mathfrak{I}^\pm(\nu, k, \rho)$ are two integrals in z of the same type, which correspond to positive and negative values of k:

$$\mathfrak{I}^\pm = \int_{-\infty}^{\infty} \frac{dz}{\sqrt{\rho^2 + z^2}}$$

$$\times \exp\left\{-i[(k \mp q)z + \sqrt{\nu(\rho^2 + z^2)}]\right\}. \tag{17}$$

Using the substitution of variable

$$\zeta = -[(k \mp q)z + \sqrt{\nu(\rho^2 + z^2)}], \tag{18}$$

we transform these integrals to

$$\mathfrak{I}^\pm = \int_{-\infty}^{\infty} \frac{e^{i\zeta} d\zeta}{\sqrt{\zeta^2 - (\nu - \nu_k^\pm)\rho^2}}, \tag{19}$$

where $\nu_k^\pm = (k \mp q)^2$.

Figure 1 for $k > 0$ schematically shows the dispersion relation for spin waves in an ideal superlattice (solid curves) in the diagram of expanded zones in the two-zone approximation. For $k = k_r = q/2$, a band gap (forbidden band) is formed in the spectrum between maximal frequency ν_1 of the first Brillouin zone and minimal frequency ν_2 of the second zone:

$$\nu_{1,2} = \nu_r \pm \Lambda_p/2, \tag{20}$$

where $\nu_r = k_r^2 \equiv (q/2)^2$ is the frequency corresponding to the center of the gap.

The dotted curve in Fig. 1 corresponds to the dispersion relation $\nu = k^2$ in the absence of the superlattice ($\Lambda_p = 0$), while the dashed curve corresponds to the auxiliary branch $\nu = \nu_k^+ \equiv (k - q)^2$.

The frequencies of the first and second Brillouin zones satisfy the inequalities $\nu < \nu_r$ and $\nu > \nu_r$, respectively. However, these frequencies (for a given k) also satisfy the inequalities $\nu < \nu_k^\pm$ and $\nu > \nu_k^\pm$, respectively. Consequently, it can be seen from formula (19) that the denominators in the integrands of integrals $\mathfrak{I}^\pm$ have different forms for the frequencies corresponding to the first Brillouin zone ($\nu < \nu_k^\pm$ for the given k) and for the frequencies corresponding to the second zone ($\nu > \nu_k^\pm$). In the former case, the denominator contains the sum of real numbers and, in accordance with formula (2.3.3.7) in the table of integrals [20], we obtain the following values of these integrals:

$$\mathfrak{I}^\pm = \int_{-\infty}^{\infty} \frac{e^{i\zeta} d\zeta}{\sqrt{\zeta^2 + a_\pm^2}} = 2K_0(a_\pm). \tag{21}$$

Here, $K_0(a_\pm)$ are the Macdonald functions, $a_\pm = \rho\sqrt{\nu_k^\pm - \nu}$, and $\mathrm{Re}\, a_\pm > 0$ in accordance with the requirements imposed on formula (2.3.3.7) [20].[1] For the second Brillouin zone ($\nu > \nu_k^\pm$), the denominator of the integrand in $\mathfrak{I}^\pm$ contains the difference of real numbers,

$$\mathfrak{I}^\pm = \int_{-\infty}^{\infty} \frac{e^{i\zeta} d\zeta}{\sqrt{\zeta^2 - b_\pm^2 \rho^2}}, \tag{22}$$

where $b_\pm = \rho\sqrt{\nu - \nu_k^\pm}$. We split each of these integrals into four integrals,

$$\int_{-\infty}^{\infty} = \int_{-\infty}^{-b} + \int_{-b}^{0} + \int_{0}^{b} + \int_{b}^{\infty}. \tag{23}$$

The sum of the first and last integrals can be transformed to one integral, which is evaluated using for-

---

[1] Pay attention to the misprint in this formula in [20] ($\sqrt{\pi}\,\Gamma(\rho)$ instead of $\sqrt{\pi}/\Gamma(\rho)$; cf. formula (2.5.6.4) in the same handbook).

mula (2.5.6.2) [20]:

$$\int_{b_\pm}^{\infty} \frac{e^{i\zeta} + e^{-i\zeta}}{\sqrt{\zeta^2 - b_\pm^2}} d\zeta = 2 \int_{b_\pm}^{\infty} \frac{d\zeta \cos\zeta}{\sqrt{\zeta^2 - b_\pm^2}} = -\pi Y_0(b_\pm), \quad (24)$$

where $Y_0(b_\pm)$ are the Neumann functions and $\mathrm{Re}\, b_\pm > 0$. The sum of the second and third integrals can be transformed analogously, and using formula (2.5.6.1) [20], we obtain

$$2 \int_0^{b_\pm} \frac{d\zeta \cos\zeta}{\sqrt{\zeta^2 - b_\pm^2}} = -i\pi J_0(b_\pm), \quad (25)$$

where $J_0(b_\pm)$ are the Bessel functions. Thus, we can write

$$\mathfrak{I}^\pm = -i\pi[J_0(b_\pm) - iY_0(b_\pm)] = -i\pi H_0^{(2)}(b_\pm), \quad (26)$$

where $H_0^{(2)}(b_\pm)$ are the Hankel functions of the second kind. Since

$$b_\pm = \rho\sqrt{\nu - \nu_k^\pm} = i\rho\sqrt{\nu_k^\pm - \nu} = ia_\pm, \quad (27)$$

we find, using the relation [21]

$$K_0(x) = -\frac{i\pi}{2} H_0^{(2)}(-ix), \quad (28)$$

that expressions (21) for integrals $\mathfrak{I}^\pm$, which were obtained for the first Brillouin zone, are also valid for the second zone, where quantities $a_\pm = \sqrt{\nu_k^\pm - \nu}$ become imaginary numbers. Therefore, expressions (22)–(28) will not be required in further analysis.

Substituting expression (21) into (15), we obtain the expressions for terms $M_p^\pm(\nu, k)$ in formula (14), which are valid for the first as well as second Brillouin zone (except in the vicinity of $k = q$ in this zone) for an arbitrary form of the decreasing part of correlation function $\mathfrak{K}(\rho)$ for 2D inhomogeneities:

$$M_p^\pm(\nu, k) = -\frac{\Lambda_p^2}{4} \int_0^\infty K_0(\rho c_\pm) \mathfrak{K}(\rho) \rho\, d\rho, \quad (29)$$

where $c_\pm = \sqrt{(k \mp q)^2 - \nu}$.

Since quantities $c_\pm$ are real-valued in the first Brillouin zone and imaginary in the second zone, expressions (29) imply that the decay associated with 2D phase inhomogeneities is not observed in the first zone and appears only in the second Brillouin zone for any form of the decrease in correlation function $\mathfrak{K}(\rho)$.

Let us find explicit expressions for $M_p^+(\nu, k)$ corresponding to different model representations of the decreasing part of correlation function $\mathfrak{K}(\rho)$.

(1) Ideal superlattice ($\gamma_2 = 0$, $\mathfrak{K}(\rho) = 1$). In accordance with formula (2.16.2.2) from the table of inte-

grals [22], relation (29) leads to the well-known expression

$$M_p^\pm(\nu, k) = \frac{\Lambda_p^2}{4} \frac{1}{\nu - (k \mp q)^2}. \quad (30)$$

(2) The most general approximation of correlation function $\mathfrak{K}(\rho)$ for 2D phase inhomogeneities is defined by expression (16). Functions $M_p^\pm(\nu, k)$ can be evaluated exactly using formula (2.16.3.14) [22]:

$$M_p^\pm(\nu, k) = -\frac{\Lambda_p^2}{4} \frac{u_\pm^{1+\gamma_2^2}}{c_\pm^2} S_{-\gamma_2^2,\, 1-\gamma_2^2}(u_\pm), \quad (31)$$

where $S_{\mu,\nu}(u_\pm)$ are the Lommel functions, $u_\pm = (e/Ck_2)c_\pm$.

(3) The particular case of correlation function (16) corresponding to $\gamma_2^2 = 1/2$. In accordance with formula (2.16.3.17) [22], functions $M_p^\pm(\nu, k)$ assume a simpler form as compared to the general case (31):

$$M_p^\pm(\nu, k) = \frac{\Lambda_p^2}{4} \frac{u_\pm}{c_\pm^2} \quad (32)$$
$$\times [\cos u_\pm \mathrm{si}(u_\pm) - \sin u_\pm \mathrm{ci}(u_\pm)],$$

where $\mathrm{si}(x)$ and $\mathrm{ci}(x)$ are integral sine and cosine, respectively.[2]

(4) Finally, let us consider the simulation of the decrease in the correlation function for 2D inhomogeneities by the exponential function

$$\mathfrak{K}(\rho) = \exp(-k_c\rho), \quad (33)$$

where effective correlation wavenumber k_c is connected with γ_2 and k_2 by the approximate relation $k_c \approx \gamma_2^2 k_2/2$. In this case, functions $M_p^\pm(\nu, k)$ can be determined by formula (2.16.6.3) [22] and, after the identity transformation, reduced to the form

$$M_p^\pm(\nu, k) = -\frac{\Lambda_p^2}{4} \frac{1}{v_\pm}\left(1 - \frac{k_c}{\sqrt{v_\pm}}\arctan\frac{\sqrt{v_\pm}}{k_c}\right), \quad (34)$$

where $v_\mp = \nu_k^\pm - \nu - k_c^2$. In contrast to formula (31) and (32), these expressions describe functions $M_p^\pm(\nu, k)$ only qualitatively because modeling correlation function (33) differs significantly from the actual function with a power asymptotic form for $\rho \longrightarrow \infty$. However, expression (34) is useful for understanding peculiarities in the effect of 2D phase inhomogeneities on the spectrum. This expression shows that 2D inhomogeneities do not result in the imaginary correction to fre-

---

[2] Pay attention to the fact that formula (2.16.3.17) in [22] contains coefficient 1/2 instead of 1/4.

quency itself even in the second Brillouin zone ($\nu > \nu_k^{\pm}$) as in the case of 1D and 3D inhomogeneities. An imaginary correction appears in the expressions in the parentheses in formula (34), which describe the modification of gap width Λ_p; therefore, it leads to a much weaker decay of the ways as compared to the 1D and 3D cases.

4. GREEN'S FUNCTION AND DENSITY OF STATES

The spectral properties of waves of different nature are studied by methods specific for each type of waves. In the case of spin waves, the high-frequency susceptibility is studied by the spin-wave resonance method in thin magnetic films as a function of constant magnetic field (or frequency) at a preset frequency (or, accordingly, for a preset magnetic field). This susceptibility has resonances at values of field or frequency corresponding to $k = k_p$, where k_p is determined by the conditions of size resonances of spin waves in a thin film. The susceptibility $\chi(\nu)$ being measured is proportional to Green's function $G(\nu)$ itself. The proportionality factor between $\chi(\nu)$ and $G(\nu)$ depends in $k = k_p$, but is independent of frequency as well as the magnetic field [23]. For the situation considered here, the Green's function for spin waves is calculated by formula (4), into which we substitute expression (12) for $M_a(\nu, k)$ and expression (14) for $M_p(\nu, k)$, in which terms $M_p^{\pm}(\nu, k)$ are defined by formula (31). For electromagnetic waves, unlike for spin waves, no methods have been developed for direct measurement of the form of the Green's function. For this reason, we will study the characteristic that can be calculated directly from the averaged Green's function and compared with the results of optical experiment; this characteristic is the 1D density of states

$$g(\omega) = \frac{1}{\pi} \int_0^q G''(\omega, k) dk. \qquad (35)$$

In this case, it is convenient to write the Green's function appearing in this expression in the form

$$G(\omega, k) = \frac{1}{(2\pi)^3} \left\{ \left[1 - \nu \gamma_3^2 P_a \right. \right.$$
$$\left. \left. - \frac{\nu}{2} \left(\frac{\Delta\varepsilon}{\varepsilon} \right)_p^2 (P_+ + P_-) \right] \nu - k^2 \right\}^{-1}, \qquad (36)$$

where $\gamma_3 = (\Delta\varepsilon)_a/\varepsilon$, and P_a, P_+, and P_- are functions of ν and k, which describe the effect of 3D amplitude inhomogeneities,

$$P_a = [(\sqrt{\nu} - ik_3)^2 - k^2]^{-1}, \quad \nu = \varepsilon(\omega/c)^2, \qquad (37)$$

and 2D phase inhomogeneities,

$$P_{\pm} = -\frac{1}{c_{\pm}^2} u_{\pm}^{1+\gamma_2^2} S_{-\gamma_2^2,\, 1-\gamma_2^2}(u_{\pm}). \qquad (38)$$

In particular cases, expression (38) can assume the form following from formulas (30), (32), and (34). Zero value of the denominator in the Green's function (36) implies that in the absence of amplitude ($\gamma_3 = 0$) and phase ($\gamma_2 = 0$) random inhomogeneities, the band gap at the boundary of the first Brillouin zone of the superlattice for electromagnetic waves is bounded by frequencies

$$\omega_{1,2} = \frac{\omega_r}{\sqrt{1 \mp \Delta\varepsilon/\sqrt{2}\varepsilon}}, \qquad (39)$$

where $\omega_r = cq/2\sqrt{\varepsilon}$.

In contrast to relevant expression (20) for spin waves, formula (39) contains the square root in the denominator. Expanding it in the case of narrow gaps ($\Delta\varepsilon/\sqrt{2}\,\varepsilon \ll 1$), we obtain

$$\omega_{1,2} \approx \omega_r \left[1 \pm \frac{1}{2\sqrt{2}} \left(\frac{\Delta\varepsilon}{\varepsilon} \right) + \frac{3}{16} \left(\frac{\Delta\varepsilon}{\varepsilon} \right)^2 \right]. \qquad (40)$$

It can be seen that in addition to gap $\Delta\omega$ emerging in the spectrum for electromagnetic waves, a displacement of the center of this gap must also be observed:

$$\Delta\omega \approx \frac{1}{\sqrt{2}} \left(\frac{\Delta\varepsilon}{\varepsilon} \right) \omega_r,$$
$$\omega_r' \approx \left[1 + \frac{3}{16} \left(\frac{\Delta\varepsilon}{\varepsilon} \right)^2 \right] \omega_r. \qquad (41)$$

Further, we will thoroughly investigate the effect of 2D phase inhomogeneities and 3D amplitude inhomogeneities on $G''(\nu)$ and the density of states in the vicinity of the band gap. However, we will first analyze the density of states for 1D and 3D phase inhomogeneities. The effect of such inhomogeneities on the dynamic susceptibility of the superlattice has been investigated comprehensively. However, the effect of 1D and 3D inhomogeneities on the 1D density of states with the help of the RSM model used here has not been studied earlier. Our results will be required for comparing with the effects associated with 2D inhomogeneities. Then we will consider the effect of 2D phase inhomogeneities alone on the spectral properties of a sinusoidal superlattice. Using the analytic expressions for the Green's function derived in this study, we can supplement and refine the results obtained in [15]. Then we will investigate the joint effect of 2D phase inhomogeneities and 3D amplitude inhomogeneities on the Green's function and density of states in the sinusoidal superlattice.
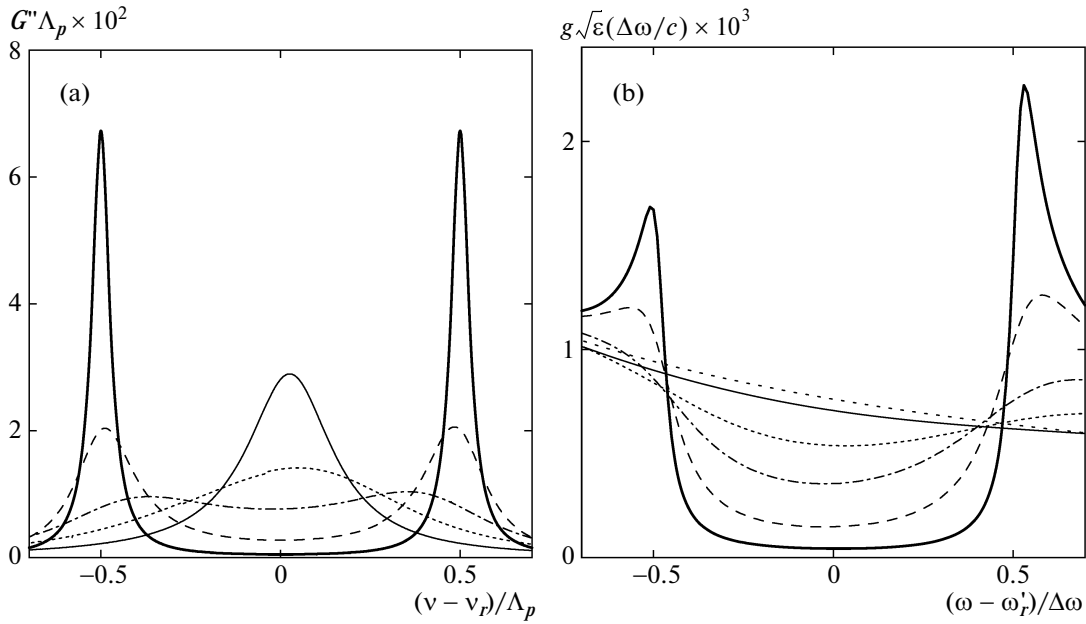
Fig. 2. (a) Effects of 1D phase inhomogeneities on Green's function $G''(\nu)$ at the boundary of the first Brillouin zone and (b) density of states $g(\omega)$ for $\kappa_1 = 1.5$ and $\gamma_1^2 = 0$ (bold solid curve), 0.3 (dashed curve), 0.1 (dot-and-dash curve), 0.2 (dotted curve), and 0.5 (fine solid curve). Rarefied-dotted curve here and in Figs. 3–5 corresponds to $g(\omega)$ for a homogeneous ferromagnet in the absence of a superlattice.
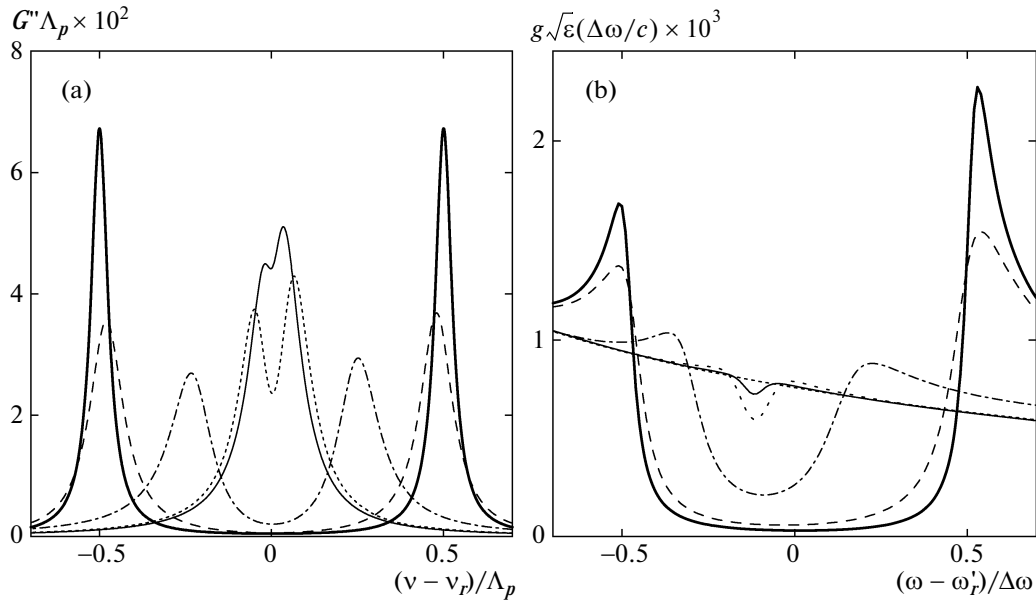
Fig. 3. (a) Effects of 3D phase inhomogeneities on Green's function $G''(\nu)$ at the boundary of the first Brillouin zone and (b) density of states $g(\omega)$ for $\kappa_3 = 1.5$ and $\gamma_3^2 = 0$ (bold solid curve), 0.08 (dashed curve), 0.5 (dot-and-dash curve), 1.5 (dotted curve), and 2.0 (fine solid curve).

4.1. 1D and 3D Phase Inhomogeneities

Figure 2 shows the dynamic susceptibility (imaginary part $G''(\nu, k)$) of the Green's function and density of states $g(\omega)$ at the boundary of the first Brillouin zone for $k = k_r = q/2$ for various values of rms fluctuations γ_1 of 1D phase inhomogeneities for a constant wavenumber of these inhomogeneities ($\kappa_1 = k_1/\sqrt{\Lambda} = 1.5$). Bold curves in Figs. 2a and 2b correspond to $\gamma_1^2 = 0$ (i.e., to an ideal superlattice). However, the peaks in
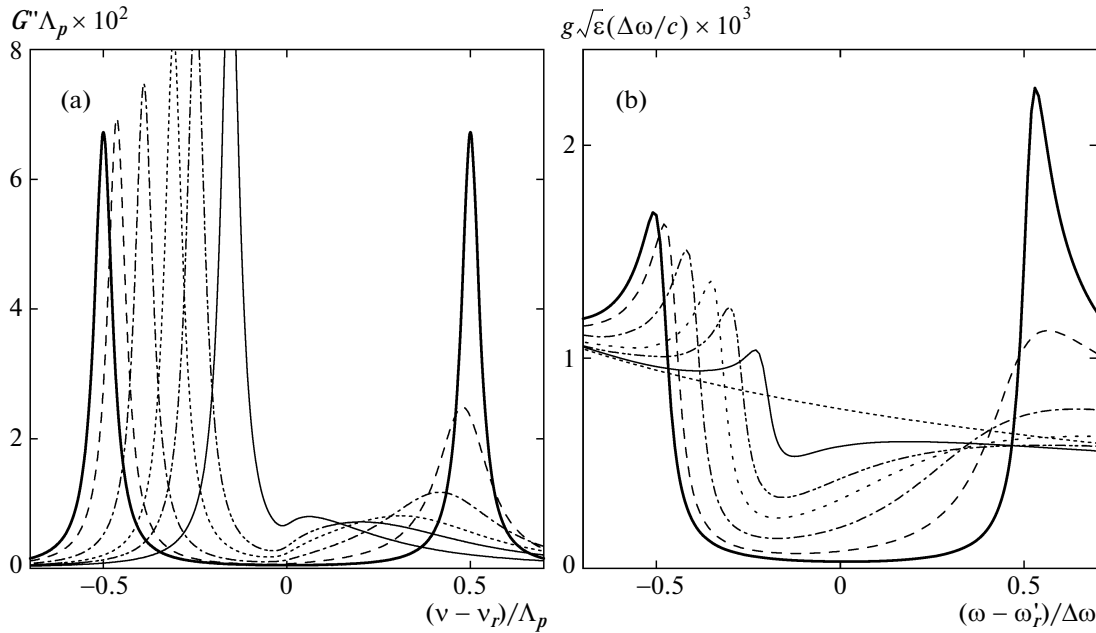
Fig. 4. (a) Green's function $G''(\nu)$ at the boundary of the first Brillouin zone of a superlattice and (b) 1D density of states $g(\omega)$ for $\kappa_2 = 1.5$ and $\gamma_2^2 = 0$ (0) (bold solid curve), 0.10 (0.15) (dashed curve), 0.33 (0.50) (dot-and-dash curve), 0.66 (1.00) (dotted curve), 1.01 (1.50) double-dash-and-dot curve, 2.01 (3.00) (fine solid curve). The values of product $\gamma_2^2 \kappa_2$ are shown in parentheses.

Fig. 2a have a finite width, and the shape of the gap in Fig. 2b differs from a rectangle because the initial decay $\nu''/\Lambda = 0.03$ has been introduced (the same refers to all the next figures). To avoid displacements of the center of the gap for the ideal superlattice, quantity $\omega - \omega_r'$, where ω_r' is defined by formula (41), is laid on the abscissa axis of this figure and all the next $g(\omega)$ graphs. It can be seen that with increasing γ_1^2, the amplitudes of both peaks decrease, while their widths increase. The peaks are slightly shifted to the center of the gap, and the interval between the peaks is filled so that a broad peaks appears at the center, which becomes narrower upon a further increase in γ_1^2. The depth of the gap in the density of states decreases with increasing γ_1^2, and the shape of the gap gradually changes from rectangular to rounded.

Figure 3 shows dependences $G''(\nu)$ and $g(\omega)$ at the boundary of the first Brillouin zone for different values of rms fluctuations γ_3^2 of 3D phase inhomogeneities for a constant value of $\kappa_3 = k_3/\sqrt{\Lambda} = 1.5$. It can be seen that the amplitude of the peaks on the $G''(\nu)$ dependence decrease with increasing γ_3^2 at a lower rate as compared to the case of 1D inhomogeneities, but at the same time, become closer quite rapidly. Accordingly, the gap in the density of states is closed due to a decrease in its depth as well as due to its quite rapid

narrowing. The center of the gap is displaced thereby towards lower frequencies. The effect of displacement of the center of the gap is typical of 1D and 3D as well as 2D inhomogeneities (see below). Our analysis has shown that the gap closing regime in the spectrum upon an increase in γ_3^2 shown in Fig. 3 corresponds to values of $\kappa_3 > 1$ only. For small values of κ_3, an increase in γ_3^2 leads to the pattern for $G''(\nu)$ as well as for $g(\omega)$), which is qualitatively similar to those in Figs. 2a and 2b corresponding to 1D inhomogeneities.

The common property of the effect of 1D and 3D inhomogeneities is the symmetry in the behavior of the left and right peaks upon an increase in the intensity of inhomogeneities.

4.2. 2D Phase Inhomogeneities

Figure 4 shows dynamic susceptibility $G''(\nu, k)$ and density of states $g(\omega)$ at the boundary of the first Brillouin zone at $k = k_r = q/2$ for different rms fluctuations γ_2 of 2D phase inhomogeneities for a constant correlation wavenumber k_2 of these inhomogeneities ($\kappa_2 = k_2/\sqrt{\Lambda_p} = 1.5$). Bold solid curves in Figs. 4a and 4b correspond to $\gamma_2^2 = 0$. It can be seen that with increasing γ_2^2, asymmetry in the behavior of low- and high-frequency peaks at the edges of the gap appears and
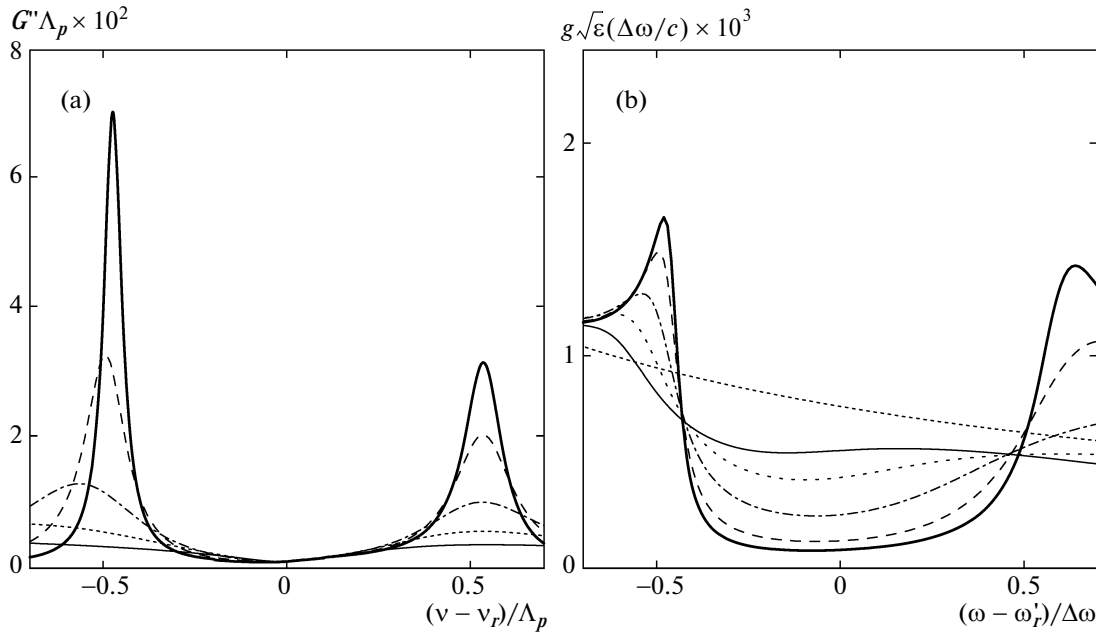
Fig. 5. Effects of 3D amplitude inhomogeneities on (a) Green's function $G''(\nu)$ and (b) on density of states $g(\omega)$ of the superlattice containing 2D phase inhomogeneities with constant characteristics $\gamma_2^2 = 0.51$ and $\kappa_2 = 0.3$. The curves correspond to $\kappa_3 = 1.0$ and $\mathscr{E}_3 = \Lambda_a / \sqrt{2} \, \Lambda_p = 0$ (bold solid curve), 0.5 (dashed curve), 1.0 (dot-and-dash curve), 1.5 (dotted curve), and 2.0 (fine solid curve).

increases. This effect, which is typical of only 2D inhomogeneities, was established for the first time in [15]. However, unlike in [15], Fig. 4a demonstrates not only the sharp decrease in the right peak, but also its displacement to the center of the band gap. The left peak also shifts to the center of the band gap. The width of the left peak remains unchanged because it is determined only by the initial decay, while the amplitude of this peak increases.

Our analysis shows that there are two modes in the behavior of the high-frequency peak upon an increase in γ_2^2, which are determined by the magnitude of dimensionless correlation wavenumber κ_2. For small values of κ_2 used in [15] ($\kappa_2 \approx 0.45$), the right peak is almost not displaced with increasing γ_2^2, when its amplitude decreases and its width increases. The second mode corresponds to values of $\kappa_2 > 1$. In this case, an increase in γ_2^2 leads to a decrease in the amplitude of the right peak and its displacement to the center of the gap. The left and right peaks become closer and merge into one peak. It can be seen from Fig. 4b that with increasing γ_2^2, the gap in the density of states becomes narrower and is deformed. The asymmetry effect is manifested in the $g(\omega)$ dependence also: the left edge of the gap remain almost vertical upon a decrease in the width and depth of the gap, while the right edge becomes inclined.

We also studied the dynamic susceptibility and the density of states at the boundary of the Brillouin zone for different values of the correlation wavenumber κ_2 of inhomogeneities for a constant value of γ_2^2. The effect of increasing asymmetry in the susceptibility peaks at the edges of the band gap is observed in this case also. The curves describing the $G(\nu)$ and $g(\omega)$ dependences, for which the values of product $\kappa_2 \gamma_2^2$ indicated in the parentheses in the caption to Fig. 4 are identical, are in qualitative agreement with the curves in Fig. 4. At first glance, this regularity is not trivial because parameters γ_2^2 and κ_2 appear in expression (31) for the mass operator of Green's function in essentially different manners: γ_2^2 appears in the exponentts of the Lommel function, while k_2 appears in the argument of this function. However, this regularity is manifested explicitly in the approximation using exponential correlation function (33), for which the effective correlation wavenumber assumes the form $k_c \approx k_2 \gamma_2^2 / 2$. In contrast to two possible modes that can be manifested upon an increase in γ_2^2, both left and right peaks are displaced to the center of the band upon an increase in κ_2 for any value of $\gamma_2^2 = \text{const}$.
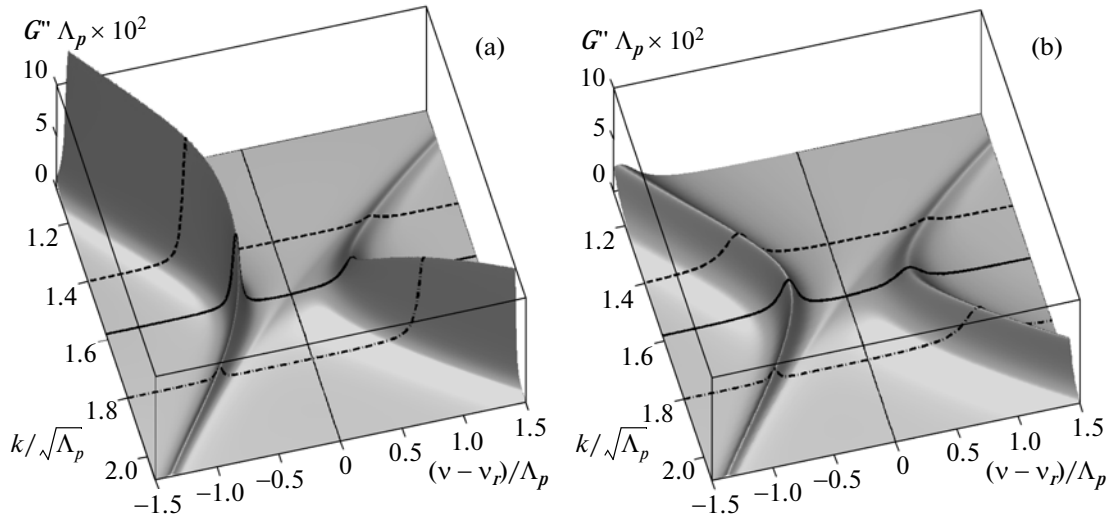
Fig. 6. (a) Schematic diagram of Green's function $G''(\nu, k)$ in the vicinity of the band gap of a superlattice in the presence of 2D phase inhomogeneities corresponding to $\kappa_c = 0.1$ and (b) variation of function $G''(\nu, k)$ after the addition of 3D amplitude inhomogeneities with $\kappa_3 = 0.5$ and $\mathscr{E}_3 = 0.4$. Cross sections of function $G''(\nu, k)$ corresponding to $k = k_r$ (solid curves), $k < k_r$ (dashed curves), and $k > k_r$ (dot-and-dash curves).

4.3. 2D Phase Inhomogeneities and 3D Amplitude Inhomogeneities

Figure 5 shows the effect of increase in rms fluctuations of 3D amplitude inhomogeneities on the dynamic susceptibility and density of states of a superlattice containing 2D phase inhomogeneities also. The magnitude of these fluctuations is characterized by parameter $\mathscr{E}_3 = \Lambda_a / \sqrt{2} \Lambda_p$. Bold solid curves in Figs. 5a and 5b correspond to the absence of 3D inhomogeneities ($\mathscr{E}_3 = 0$) and describe the asymmetry effect due to 2D phase inhomogeneities with constant characteristics ($\gamma_2 = 0.5$ and $\kappa_2 = 0.3$). It can be seen from Fig. 5a that an increase in fluctuations of 3D inhomogeneities leads to a decrease in the amplitudes of both dynamic susceptibility peaks. However, the rate of the decrease in the height of the left peak exceeds the rate of the decrease in the height of the right peak. As a result, the amplitudes and widths of the peaks are leveled out, and the asymmetry effect associated with 2D inhomogeneities disappears. Figure 5b shows that an enhancement of fluctuations in 3D amplitude inhomogeneities leads to a decrease in the gap depth and a slight broadening of the gap in the density of states. In this case, the gap remains asymmetric.

Figure 6 shows the spatial diagram of the imaginary part $G''(\nu, k)$ of the Green's function in the vicinity of the gap between the first and second Brillouin zones. Figure 6a corresponds to the presence of only 2D phase fluctuations, while Fig. 6b illustrates the joint effect of 2D phase and 3D amplitude inhomogeneities. In plotting these graphs, we used instead of exact expression (31) for $M_p^{\pm}(\nu, k)$ approximate expression (34) corresponding to exponentially

decreasing correlation function (33). Analysis shows that the qualitative behavior of function $G''(\nu, k)$ remains the same as in the case when exact expressions for $M_p^{\pm}(\nu, k)$ are used, but the calculations are simplified significantly. The finiteness of the amplitude of function G'' in the first Brillouin zone is due to the introduction of initial decay $\nu''/\Lambda_p = 0.03$. It can be seen from Fig. 6a that the amplitude of function $G''(\nu, k)$ for the given parameters ($\kappa_c \approx \gamma_2 k_2/2 = 0.1$) decreases only insignificantly towards the band boundary $k = k_r$ upon an increase in k in the first Brillouin zone. In the second zone, the amplitude of function $G''(\nu, k)$ at $k = k_r$ is much smaller than in the first zone and increases with k. The addition of 3D amplitude inhomogeneities reduces the amplitudes of function $G''(\nu, k)$ both in the first and in the second Brillouin zones and suppresses the asymmetry effects in the amplitudes of these peaks at the edges of the band gap. Figures 6a and 6b show that the asymmetry effects for the peaks of the Green's function under the action of 2D phase inhomogeneities is clearly manifested only for exact tuning of wavenumber k to boundary k_r of the Brillouin zone. For $k < k_r$, the amplitudes of the peaks in the $G''(\nu)$ dependence are first leveled out, after which the amplitude of the high-frequency peak becomes larger than the amplitude of the low-frequency peak. For $k > k_r$, the asymmetry effect is enhanced, but this does not indicate the presence of precisely 2D inhomogeneities because this effect is observed for inhomogeneities of any dimensionality.

5. CONCLUSIONS

In this study, the Bourret approximation is used for deriving an analytic expression for averaged Green's function $G(\nu, k)$ of an initially sinusoidal superlattice with 2D phase inhomogeneities simulating random in-phase deformations of the interfaces between the layers of the superlattice. The expression derived here is valid for the first and second Brillouin zones of the superlattice except in the neighborhood of the boundary of the second zone. This enabled us to study the dynamic susceptibility and one-dimensional density of states of the superlattice with 2D phase inhomogeneities as well as with 2D phase inhomogeneities coexisting with 3D amplitude inhomogeneities, the latter inhomogeneities simulating the inhomogeneities in the material of the layers in the superlattice. It is shown that the absence of decay in the first Brillouin zone and its emergence in the second zone predicted in [4] are observed for any form of the decay in the correlation function for 2D phase inhomogeneities.

It is shown that the asymmetry effect in the amplitudes of the dynamic susceptibility peaks at the edges of the band gap in the spectrum of the superlattice upon an increase of rms fluctuations γ_2 of 2D inhomogeneities, which was predicted in [15] as typical of only 2D phase inhomogeneities, is also observed upon an increase in correlation wavenumber κ_2 of such inhomogeneities. Detailed analysis of the asymmetry effect has shown that in the case of an increase in γ_2 for $\kappa_2 =$ const, the closure of the gap in the spectrum can proceed in accordance with two different modes depending on the value of κ_2. In both modes, the height of the low-frequency peak slightly increases, while the height of the high-frequency peak sharply decreases upon an increase in γ_2. However, for small values of κ_2 ($\kappa_2 < 0.5$), the low-frequency peak is displaced to the center of the band gap, while the high-frequency peak does not change its position. It is this mode that was studied in [15, 16].

In this study, we considered the second mode observed for $\kappa_2 > 1$. In this mode, equally strong asymmetry in the peak heights is accompanied by almost symmetrical displacements of both peaks to the center of the band gap. If the value of κ_2 increases for $\gamma_2 =$ const, it is only this latter mode that is manifested for all values of γ_2 investigated here. The asymmetry effect is also manifested in the shape of the 1D density of states: the left edge of the gap remains almost vertical, while the right edge becomes inclined. It is shown that for different and not very small values of κ_2 and γ_2^2, the dynamic susceptibility curves, as well as the curves describing the density of states and corresponding to the same value of product $\kappa_2\gamma_2^2$ are similar both qualitatively and quantitatively.

We have analyzed the effect of 3D amplitude inhomogeneities on the dynamic susceptibility and density of states of a superlattice containing 2D phase inhomogeneities. An increase in the rms fluctuations of 3D inhomogeneities leads to a decrease in the dynamic susceptibility peak amplitudes in both Brillouin zones. It is shown that the rate of decrease in the amplitude of the low-frequency peak at the edge of the gap in the superlattice spectrum exceeds the rate of the decrease in the amplitude of the high-frequency peak. As a result, the amplitudes and widths of both peaks are leveled out, and the asymmetry effect associated with 2D inhomogeneities is suppressed. An increase in fluctuations of 3D amplitude inhomogeneities reduces the depth of the gap in the density of states in the region of the band gap. The gap is slightly broadened in this case.

Thus, in contrast to phase and amplitude inhomogeneities of other dimensionalities, 2D phase inhomogeneities describing in-phase deformations of all interfaces between the layers of a superlattice lead to the asymmetry effect in the dynamic susceptibility and in the density of states at the boundary of the Brillouin zone of the superlattice. Such effects can be observed experimentally in magnetic and optical superlattices. It should be borne in mind that in analyzing dynamic susceptibility by the spin-wave resonance method, the asymmetry effects associated with correlations between interfaces are manifested only when one of resonant wavenumbers k_n coincides with the wavenumber corresponding to the Brillouin zone boundary of the superlattice. If this condition is violated, asymmetry emerging in the dynamic susceptibility can be due to other factors.

Targeted experiments on observation of the effect studied here and in [4, 15, 16] would facilitate the development of radio-spectroscopy and optical methods for identifying the presence of mutual correlations between inhomogeneities in various interfaces in superlattices. Such experiments should be performed in complex with experiments on small-angle X-ray scattering on the same samples. In the presence of long-range correlations between roughnesses in interfaces (2D phase inhomogeneities), radio-spectroscopy or optical methods can reveal additional decay in the second Brillouin zone of the superlattice and asymmetry in the susceptibility peaks and in the density of states at the Brillouin zone boundary, while small-angle scattering technique will make it possible to observe the resonance effects in the diffuse region of the X-ray scattering spectra, which were studied in detail theoretically, as well as the characteristic distribution of intensity strips on the $k_x k_z$ plane of wavevectors [11−14].

ACKNOWLEDGMENTS

"Development of the Higher School Scientific Potential" in 2009−2010 and 2011 years.

REFERENCES

1. N. Nishiguchi, S. Tamura, and F. Nori, Phys. Rev. B: Condens. Matter **48**, 2515 (1993).

2. T. Gruner and D.-G. Welsch, Phys. Rev. A: At., Mol., Opt. Phys. **54**, 1661 (1996).

3. Yunxia Dong and Xiangdong Zhang, Opt. Express **16**, 16950 (2008).

4. V. A. Ignatchenko and Yu. I. Mankov, Phys. Rev. B: Condens. Matter **56**, 194 (1997).

5. A. N. Malakhov, Sov. Phys. JETP **3**, 701 (1956).

6. S. M. Rytov, *Introduction to the Statistical Radiophysics* (Nauka, Moscow, 1976), Part 1 [in Russian].

7. V. A. Ignatchenko, Yu. I. Mankov, and A. A. Maradudin, J. Phys.: Condens. Matter **11**, 2773 (1999).

8. V. A. Ignatchenko, Yu. I. Mankov, and A. A. Maradudin, Phys. Rev. B: Condens. Matter **68**, 024209 (2003).

9. V. A. Ignatchenko and Yu. I. Mankov, Phys. Rev. B: Condens. Matter **75**, 235422 (2007).

10. S. K. Sinha, E. B. Sirota, S. Garoff, and H. B. Stanley, Phys. Rev. B: Condens. Matter **38**, 2297 (1988).

11. R. L. Headrick and J.-M. Baribeau, Phys. Rev. B: Condens. Matter **48**, 9174 (1993).

12. V. Holý and T. Baumbach, Phys. Rev. B: Condens. Matter **49**, 10668 (1994).

13. E. A. Kondrashkina, S. A. Stepanov, R. Opitz, M. Schmidbauer, R. Köhler, R. Hey, M. Wassermeier, and D. V. Novikov Phys. Rev. B: Condens. Matter **56**, 10469 (1997).

14. V. Holý, J. Mater. Sci.: Mater. Electron. **10**, 223 (1999).

15. V. A. Ignatchenko, Yu. I. Mankov, and D. S. Tsikalov, JETP **107** (4), 603 (2008).

16. Yu. I. Mankov and D. S. Tsikalov, Phys. Solid State **52** (3), 544 (2010).

17. R. C. Bourret, Nuovo Cimento **26**, 1 (1962); Can. J. Phys. **40**, 782 (1962).

18. V. A. Ignatchenko, A. A. Maradudin, and A. V. Pozdnaykov, Phys. Met. Metallogr. **91** (Suppl. 1), S69 (2001).

19. V. A. Ignatchenko and R. S. Iskhakov, Sov. Phys. JETP **45** (3), 526 (1977).

20. A. P. Prudnikov, Yu. A. Brychkov, and O. I. Marichev, *Integrals and Series*, Vol. 1: *Elementary Functions* (Nauka, Moscow, 1981; Gordon and Breach, New York, 1986).

21. E. Jahnke, F. Emde, and F. Lösch, *Tafeln höherer Funktionen* (Teubner, Stuttgart, Germany, 1960; Nauka, Moscow, 1964) [in German and in Russian].

22. A. P. Prudnikov, Yu. A. Brychkov, and O. I. Marichev, *Integrals and Series*, Vol. 2: *Special Functions* (Nauka, Moscow, 1983; Gordon and Breach, New York, 1990).

23. V. A. Ignatchenko, Yu. I. Man'kov, and A. V. Pozdnyakov, JETP **89** (4), 717 (1999).

Translated by N. Wadhwa